RESEARCH

Effects of La$_2$O$_3$ mass fraction on microstructure and friction-wear performances of WC − 10Co4Cr − Al$_2$O$_3$ coatings by laser cladding

Shi Jiangzheng[1] · Kong Dejun[1]

Abstract

In order to improve the hardness and wear resistance of cold work molds, La$_2$O$_3$-reinforced WC − 10Co4Cr − Al$_2$O$_3$ coatings were fabricated on Cr12MoV steel by laser cladding (LC). The morphologies, grain sizes, and phases of obtained coatings were analyzed using a digital microscopic system (DMS) and X-ray diffraction (XRD), respectively. The effects of La$_2$O$_3$ mass fraction on the tribological performance and wear mechanism of WC − 10Co4Cr − Al$_2$O$_3$ coatings were analyzed using a ball-on-disk wear tester. The results show that the La$_2$O$_3$-reinforced WC − 10Co4Cr − Al$_2$O$_3$ coatings are composed of WC, W$_2$C, Al$_2$O$_3$, La$_2$O$_3$, LaAlO$_3$, and Fe − Cr, AlP$_3$Si, LaCoO$_3$, and LaP phases, and the hardness of obtained coatings increases with the increase of La$_2$O$_3$ mass fraction. The average coefficients of friction (COFs) of WC − 10Co4Cr − Al$_2$O$_3$ − 3%La$_2$O$_3$, − 6%La$_2$O$_3$, and − 9%La$_2$O$_3$ coatings are 0.57, 0.52, and 0.46, respectively; and the corresponding wear rates are 63.18, 47.1, and 27.99 μm^3•s^{-1}•N^{-1}, showing that the friction reduction and wear resistance of WC − 10Co4Cr − Al$_2$O$_3$ − 9%La$_2$O$_3$ coating are the best among the three kinds of coatings, and the grain refinement and dispersion strengthening by the addition of La$_2$O$_3$ are the main factor affecting its wear resistance.

Keywords Laser cladding (LC) · WC − 10Co4Cr − Al$_2$O$_3$ coating · La$_2$O$_3$ mass fraction · Coefficient of friction (COF) · Wear mechanism

Introduction

As one kind of cold work mold steel, Cr12MoV steel is widely used in mold industry [1]. However, it easily occurs the wear phenomena on the mold surface during the mechanical part formations, leading to the premature failure of cold work mold. In order to increase the wear resistance of Cr12MoV steel, coating technology is applied to its surface modification. At present, the coating fabrication methods mainly include plasma spraying, high velocity oxy fuel (HVOF) spraying, and laser cladding (LC). Among them, LC is an advance method to enhance the wear resistance for mold surfaces due to its advantages of low dilution ratio, low porosity, and compact structure [2, 3].

In the past few decades, Co-based WC coatings with high hardness and wear resistance have been paid attentions [4, 5]. Song et al. [6] investigated the dry-sliding wear performances of WC − CoCr and WC − Cr$_x$C$_y$ − Ni coatings by HVOF, showing that the COF and wear rate of WC − CoCr coating are less than those of WC − Cr$_x$C$_y$ − Ni coating. And Voorwald et al. [7] compared the wear resistances of WC − 17Co and WC − 10Co4Cr coatings prepared by HVOF with the hard Cr plating coating, and revealed that the wear resistance of WC − 10Co4Cr was higher than those of WC − 17Co and hard Cr plating coating. The above analyses show that the WC − 10Co4Cr coating presents an outstanding wear resistance, which is widely applied in the surface modification of mold steel.

In earlier studies, dry-sliding friction performance of laser-cladded WC − 10Co4Cr coating with different Al$_2$O$_3$ mass fractions was reported [8], and found that the COFs and wear rates of WC − 10Co4Cr coatings reduced with the increase of Al$_2$O$_3$ mass fraction. Moreover, to further enhance the hardness and wear performance of WC − 10Co4Cr coating, many studies have shown that rare earth oxides such as CeO$_2$, La$_2$O$_3$, and Y$_2$O$_3$ [9–11] are commonly added to the coatings. Sharma et al. [12] revealed that the incorporation of La$_2$O$_3$ in the WC-based coating enhanced its hardness and wear resistance due to the effect

✉ Kong Dejun
kong-dejun@163.com

[1] School of Mechanical Engineering, Changzhou University, Changzhou 213164, People's Republic of China

of refinement strengthening. Wang et al. [13] found that the addition of La_2O_3 reduced the COFs and improved the wear resistance of WC–Ni coatings. The above results showed that adding La_2O_3 could improve the wear resistance of WC-based coating. However, the effects of La_2O_3 mass fraction on the friction-wear performance of $WC - 10Co4Cr - Al_2O_3$ coating on Cr12MoV steel have rarely reported, which is a promising method to improve the wear resistance of WC-based coatings on the cold work molds.

In this study, $WC - 10Co4Cr - Al_2O_3$ coatings with the different La_2O_3 mass fractions were fabricated on Cr12MoV steel by LC. The aim was to investigate the influence of La_2O_3 mass fraction on the microstructure, hardness, COFs, and wear rates of $WC - 10Co4Cr - Al_2O_3$ coatings, and the wear mechanism was also discussed, which provided a reference for the surface modification of Cr12MoV steel.

Experimental procedures

Sample preparations

The substrate was Cr12MoV cold work mold steel, which was derusted and roughened with the sandblasting treatment to increase its surface activity [14], and then cleaned with alcohol for the coating fabrication. The $WC - 10Co4Cr$ and Al_2O_3 powder with the size of 15–45 μm (Beikuang New Materials Technology Co., Ltd.) and the La_2O_3 powder with the size of 1–15 μm (Hebei Bocheng metallurgical center) were used as raw materials. The laser cladding powders of $WC10Co4Cr - 6\%Al_2O_3 - 3\%La_2O_3, - 6\%Al_2O_3 - 6\%La_2O_3$, and $- 6\%Al_2O_3 - 9\%La_2O_3$ were mixed on a QM3SP04L type planetary ball miller to obtain the uniformly mixed powder [15]. Technological parameters: mass ratio of mixed powders and ZrO_2 balls were 1:10; rotation speed of 500 r/min; and mixing time of 5 h.

The LC test was conducted on a $ZKSX - 2008$ type fiber-coupled LC system with the $DPSF - 3$ type negative pressure powder feeder, where the lateral powder feeding and multi-pass overlap methods [8] were used to fabricate the coatings, as shown in Fig. 1. Technological parameters are as follows: laser power of 1500 W; laser spot of 4 mm; scanning speed of 2 mm/s; powder feeding speed of 11 mL/min; and overlap ratio of 50%.

After the LC test, the sample was cut into the dimension of $15 \times 15 \times 5$ mm by wire electrical discharge machine, and the coatings' surface and cross-section were polished to a mirror on a metallographic polishing machine.

Characterization methods

The microstructure of obtained coatings was analyzed using a $VHX - 700FC$ type digital microscopic system (DMS),

1–Touch screen
2–Optical fiber
3–Solid state fiber coupled output laser
4–Laser emitter
5–Laser beam
6–Argon atmosphere
7–Coating
8–Substrate

9–Molten pool
10–Powder
11–Nozzle
12–Powder feeding pipe
13–Negative pressure powder feeder
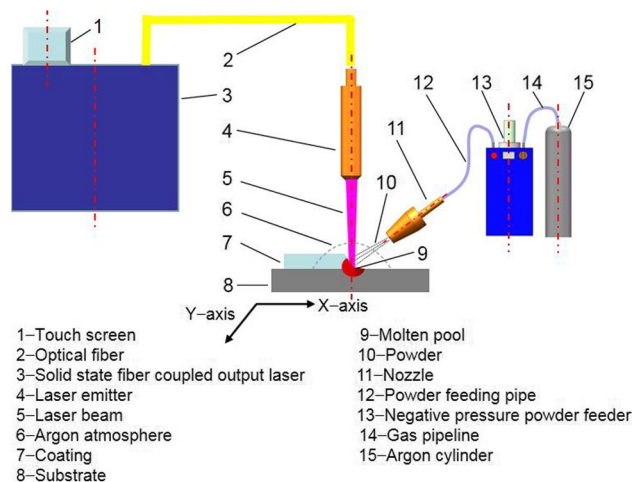14–Gas pipeline
15–Argon cylinder

Fig.1 Sketch of laser cladding with lateral powder feeding

which were corroded by alcohol solution with the 5% nitric acid (volume fraction). The grain size was measured using a DMS, which was accorded with the intersection method [16]. The phases were analyzed using a D/max 2500PC type X-ray diffraction (XRD) with the X-ray source of Cu target, and the range of 2 − theta was at 20–90°. The coating porosity was presented with the average values in the five sampling areas, which was measured using an Image-J software with the thresholding technique [17].

The hardness was measured using a $HXD - 1000$ type microhardness tester, and test parameters: load of 10 N; and holding time of 10 s. The friction-wear test was conducted on a $CFT - I$ type comprehensive performance test with the sliding friction method at room temperature [18], and test parameters: tribo-pair of Si_3N_4 ball with diameter of 3 mm [19]; load of 6 N [6, 20, 21]; running length of 4 mm; reciprocating speed of 200 times/min; and sliding time of 60 min [22, 23]. After the wear test, the profiles, morphologies, and chemical elements of worn tracks were analyzed using a DMS, SEM, and its configured electron energy spectrometer (EDS), respectively. The wear model was built to discuss the wear mechanism of La_2O_3-reinforced $WC10Co4Cr - Al_2O_3$ coating, and the role of La_2O_3 in the friction reduction and wear resistance process was also analyzed in detail.

Result analysis and discussion

Morphologies and XRD analysis of powder

Figure 2(a) shows the morphology of $WC - 10Co4Cr$ powder. The powder with the spherical shape had good fluidity in the conveying pipe, and its high specific surface was conducive to the formation of dense coating [24]. Figure 2(b) shows the morphology of Al_2O_3 powder. The powder with

Fig.2 Morphologies of
$WC - 10Co4Cr$, Al_2O_3, and
La_2O_3 powders and XRD analy-
sis of mixed powders

(a) WC−10Co4Cr powder

(b) Al$_2$O$_3$ powder

(c) La$_2$O$_3$ powder

(d) XRD patterns of mixed powders
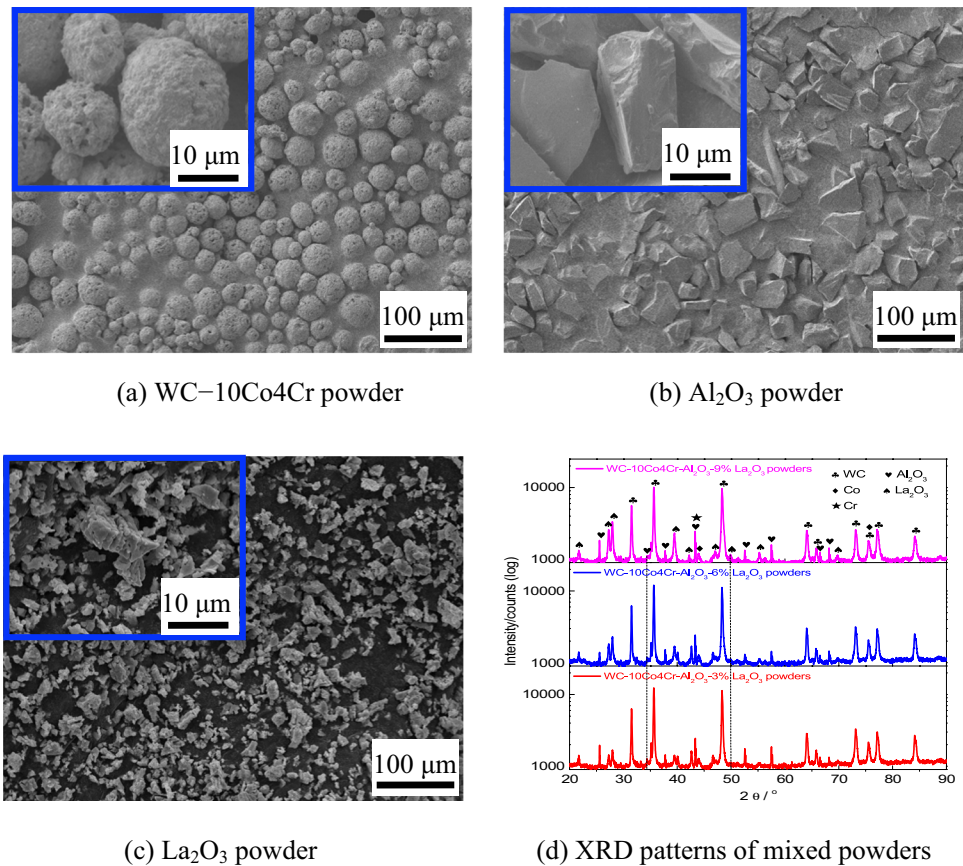
the angular and blocky shape had stronger embedding capa-
bility in the coating, which improved its wear resistance
[25]. Figure 2(c) shows the morphology of La_2O_3 powder.
The powder was sheet structure with good lubrication, which
effectively reduced the COF and improved the wear resist-
ance of coating [26]. Figure 2(d) shows the XRD analy-
sis of $WC - 10Co4Cr - Al_2O_3$ and La_2O_3 mixed powders.
The powders were composed of WC (PDF# $51 - 0939$),
Co (PDF# $15 - 0806$), Cr (PDF# $19 - 0323$), Al_2O_3 (PDF#
$88 - 0826$), and La_2O_3 (PDF# $54 - 0213$) phases, where the
WC was the main phase. No new phases appeared, suggest-
ing that the La_2O_3 mass fraction had little effects on the
phase compositions of mixed powders after the ball-milling
process.

## Characterization and analysis of coatings

Microstructure, porosity, and phases of coating surfaces

The columnar grains and fine-grained dendrites were
found on the $WC - 10Co4Cr - Al_2O_3 - 3\%La_2O_3$ coating,
and there were many flocculent structures, as shown in
Fig. 3(a). The $WC - 10Co4Cr - Al_2O_3 - 6\%La_2O_3$ coating
was mainly columnar grains and equiaxed grains, where
the number of flocculent structure was reduced, as shown

in Fig. 3(b). Figure 3(c) shows that the microstructure of
$WC - 10Co4Cr - Al_2O_3 - 9\%La_2O_3$ coating surface was
mainly fine dispersed and uniform equiaxed grains, and
the number of flocculent structure was the least. The grain
sizes of $WC - 10Co4Cr - Al_2O_3 - 3\%La_2O_3$, $- 6\%La_2$
O_3, and $- 9\%La_2O_3$ coating surfaces were 4.23, 3.51, and
3.26 μm, respectively, showing that the grain sizes of coat-
ings decreased with the increase of La_2O_3 mass fraction.
This was because the La_2O_3 was easily gathered on the grain
boundaries, dislocations, and other defects, which produced
pinning and dragging effects [27, 28] to hinder the grain
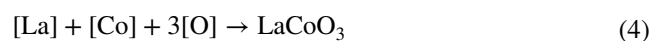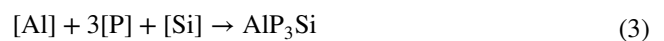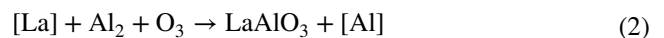growth [29].

In this case, the porosity of $WC - 10Co4Cr - Al_2O_3 - 3$
$\%La_2O_3$, $- 6\%La_2O_3$, and $- 9\%La_2O_3$ coating surfaces was
$0.53 \pm 0.15\%$, $0.34 \pm 0.12\%$, and $0.17 \pm 0.08\%$, respectively,
which decreased with the increase of La_2O_3 mass fraction.
This was because the addition of La_2O_3 reduced the interfa-
cial tension of melting pool, which improved its wettability
and fluidity [30]. Therefore, the capability of liquid-phase
filling the pores was enhanced, which caused the gas easily
escape and reduced the coating porosity.

Figure 4 shows the XRD patterns of $WC - 10Co4Cr - Al_2O_3$
coatings with different La_2O_3 mass fractions. The La_2O_3 rein-
forced $WC - 10Co4Cr - Al_2O_3$ coatings were mainly com-
posed of WC (PDF# $65 - 4539$), W_2C (PDF# $35 - 0776$),
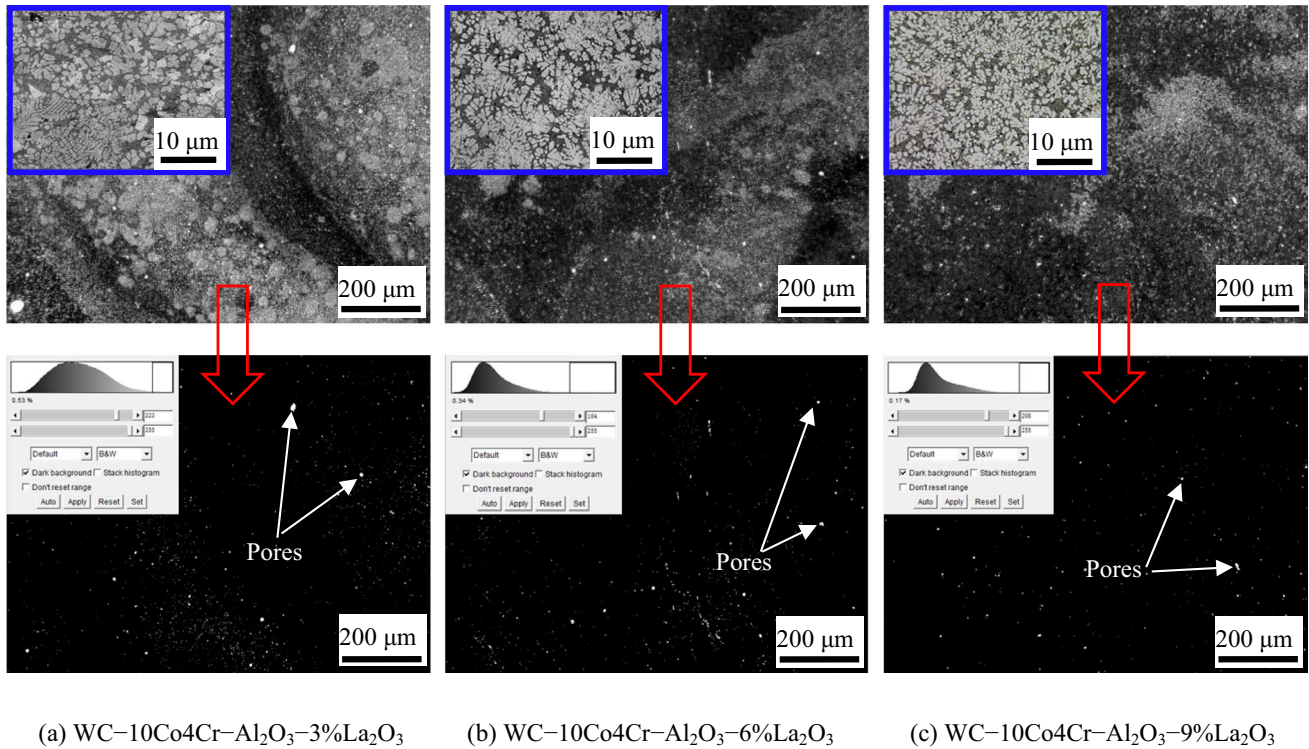
(a) WC−10Co4Cr−Al$_2$O$_3$−3%La$_2$O$_3$ (b) WC−10Co4Cr−Al$_2$O$_3$−6%La$_2$O$_3$ (c) WC−10Co4Cr−Al$_2$O$_3$−9%La$_2$O$_3$

Fig.3 Microstructure and porosity of WC − 10Co4Cr − Al$_2$O$_3$ coating surface with different La$_2$O$_3$ mass fractions
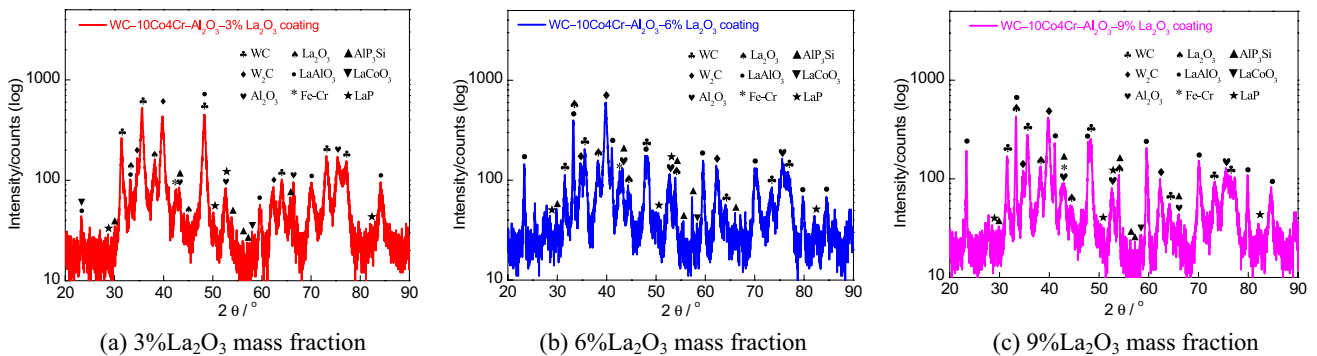
(a) 3%La$_2$O$_3$ mass fraction   (b) 6%La$_2$O$_3$ mass fraction   (c) 9%La$_2$O$_3$ mass fraction

Fig.4 XRD analysis of WC − 10Co4Cr − Al$_2$O$_3$ coatings with different La$_2$O$_3$ mass fractions

Al$_2$O$_3$ (PDF# 23 − 1009), La$_2$O$_3$ (PDF# 24 − 0554), LaAlO$_3$ (PDF# 85 − 1071), Fe − Cr (PDF# 34 − 0396), AlP$_3$Si (PDF# 35 − 1041), LaCoO$_3$ (PDF# 06 − 0491), and LaP (PDF# 18 − 0682) phases. In this case, the W$_2$C originated from the decarburization of WC during the LC test [8]. The Fe − Cr had two sources, i.e., (1) the combination of Cr and Fe in the melting pool [31] and (2) the Fe − Cr phases in the substrate flowed from the substrate to coating in the LC process [32]. The LaAlO$_3$ compound came from the reaction product of La$_2$O$_3$ with the Al$_2$O$_3$ [33, 34]. In addition, a part of La and Al were reduced by the La-formed new compounds with the O, Co, Si, P, and other elements in the melting pool, such as

AlP$_3$Si, LaCoO$_3$, and LaP compounds [12, 35, 36]. The reaction processes were shown as follows:

$$La_2O_3 + 3[C] \rightarrow 2[La] + 3CO \tag{1}$$

$$[La] + Al_2 + O_3 \rightarrow LaAlO_3 + [Al] \tag{2}$$

$$[Al] + 3[P] + [Si] \rightarrow AlP_3Si \tag{3}$$

$$[La] + [Co] + 3[O] \rightarrow LaCoO_3 \tag{4}$$

$$[La] + [P] \rightarrow LaP \tag{5}$$

Microstructure and porosity of coating cross-sections

The images and porosity of $WC-10Co4Cr-Al_2O_3$ coating cross-sections with the different La_2O_3 mass fractions are shown in Fig. 5. The coating cross-sections with the thicknesses of ~ 1 mm were smooth, with no significant cracks. There were a wavy bonding zone formed at the coating interface, and the substrate had obvious deformation, resulting in the increase of effective bonding zone between the coating and the substrate [37]. The porosity of $WC-10Co4Cr-Al_2O_3-$ $3\%La_2O_3, -6\%La_2O_3,$ and $-9\%La_2O_3$ coating cross-sections was $0.89\pm0.14\%$, $0.71\pm0.11\%$, and $0.58\pm0.12\%$, respectively, showing that the porosity decreased with the increase of La_2O_3 mass fraction.

In order to investigate the details of constituent and microstructural features of coatings, the images of coating cross-section were extracted from the different regions along the depth direction of $WC-10Co4Cr-Al_2O_3 - La_2O_3$ coatings. Figure 5(a1)–(c1), (a2)–(c2), and (a3)–(c3) represents the high-magnified microstructure on the coating top, middle, and bottom regions, respectively. The grains on the coating top region with dominantly columnar grains and equiaxed grains are shown in Fig. 5(a1)–(c1). The microstructure on the coating middle region in Fig. 5(a2)–(c2) were mainly columnar grains and slender dendrites, while that on the coating bottom region in Fig. 5(a3)–(c3) was mainly dominated by the slender dendrites.

Hardness of coating surfaces

Figure 6 shows that the hardness of $WC-10Co4Cr-Al_2O_3-$ $3\%La_2O_3, -6\%La_2O_3,$ and $-9\%La_2O_3$ coating surfaces were 1697 ± 21, 1751 ± 32, and 1820 ± 27 $HV_{0.5}$, respectively, which were higher than that of $WC-10Co4Cr-6\%Al_2O_3$ coating (1665 $HV_{0.5}$ [8]). The increase of hardness was mainly related to the refinement and dispersion strengthening by the addition of La_2O_3 [38]. In this case, the addition of La_2O_3 played two roles; i.e., (1) La_2O_3 was easily gathered on the grain boundaries, dislocations, and other defects, which produced pinning effects to cause the lattice distortion and hinder the movement of dislocations [39]; and (2) the porosity and average grain sizes of coatings gradually decreased with the increase of La_2O_3 mass fraction, which improved the coating hardness.

Friction-wear performances

COFs and wear rates

Figure 7(a) shows the COFs vs wear time of $WC-10Co4Cr-Al_2O_3$ coatings with the different La_2O_3

mass fractions. The average COFs of $WC-10Co4Cr-Al_2O_3-3\%La_2O_3, -6\%La_2O_3,$ and $-9\%La_2O_3$ coatings were 0.57, 0.52, and 0.46, respectively, indicating that the addition of La_2O_3 significantly reduced the COFs of coatings. The wear process was divided into the running-in and the normal wear periods [40], where the time of running-in period was shortened with the increase of La_2O_3 mass fraction. In the running-in friction process, the temperature of contact point increased with the friction time, and the La_2O_3 with the lubrication effect [26] was beneficial to reducing the coating COFs. Moreover, the addition of La_2O_3 easily formed an oxide film on the coating surface [41], which was destroyed and became fine abrasive debris with the continuous wear of worn track to reduce the COFs.

Figure 7(b) and (c) shows the profiles of worn tracks and wear rates of $WC-10Co4Cr-Al_2O_3$ coatings with the different La_2O_3 mass fractions. The wear volumes of $WC-10Co4Cr-Al_2O_3-3\%La_2O_3, -6\%La_2O_3,$ and $-9\%La_2O_3$ coatings were 1.36×10^6, 1.02×10^6, and 6.05×10^5 μm^3, respectively; and the corresponding wear rates were 63.18, 47.1, and 27.99 $\mu m^3 \bullet s^{-1} \bullet N^{-1}$, respectively, indicating that the wear resistance of $WC-10Co4Cr-Al_2O_3$ coating was effectively enhanced with the increase of La_2O_3 mass fraction. Generally, the wear resistance of coating was positively related to its porosity [42], and the relationship was showed as follows:

$$K = K_0 \exp(-23\rho) \tag{6}$$

where K was the wear rate of porous coating/$N\bullet m/mm^3$; K_0 was the wear rate of coating without pores/$N\bullet m/mm^3$; and ρ was the porosity of coating/%.

According to the Eq. (6), it was known that the low porosity of coating meant the high wear resistance. It was suggested that the $WC-10Co4Cr-Al_2O_3-9\%La_2O_3$ coating had the lowest wear rate among the three kinds of coatings, which was because the coating with high oxide content usually had high hardness [43, 44]. Besides, the hard phases were more evenly distributed on the coating with the increase of La_2O_3 mass fraction, and the effect of grain refinement was more obvious, which played the strengthening roles of dispersion and grain refinement.

Morphologies of worn tracks

The overall images of worn tracks on the $WC-10Co4Cr-Al_2O_3$ coatings with the different La_2O_3 mass fractions are shown in Fig. 8. The widths of worn tracks on the $WC-10Co4Cr-Al_2O_3-3\%La_2O_3, -6\%La_2 O_3,$ and $-9\%La_2O_3$ coatings declined with the increase of La_2O_3 mass fraction, and the surfaces of worn tracks also became smoother, indicating that the wear and spalling was reduced with the increase of La_2O_3 mass fraction.

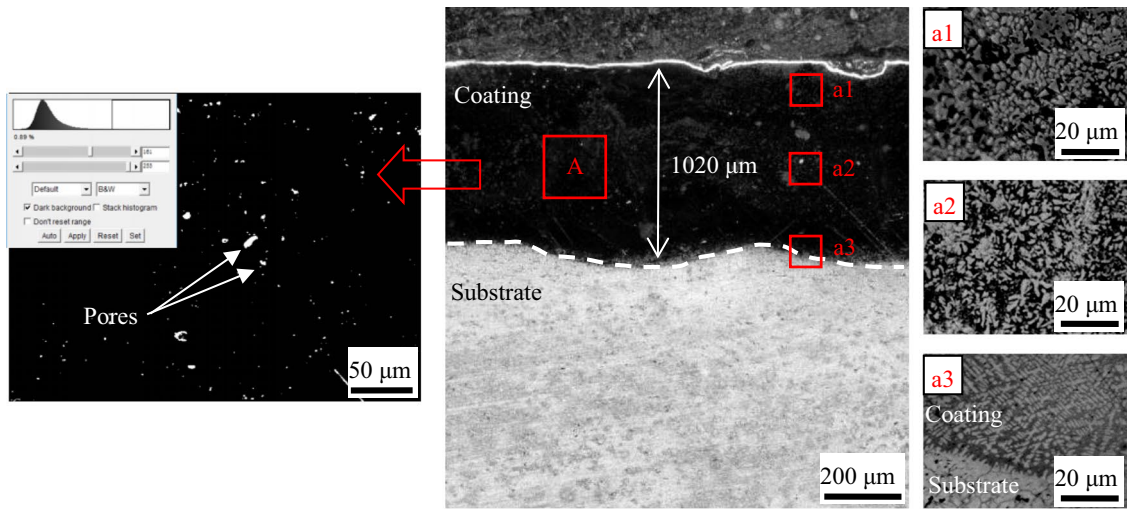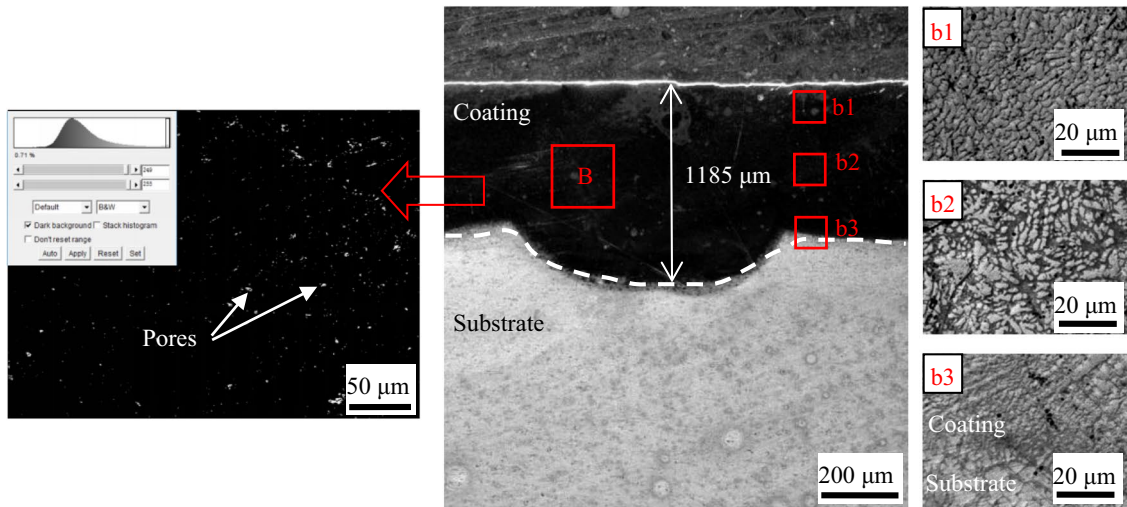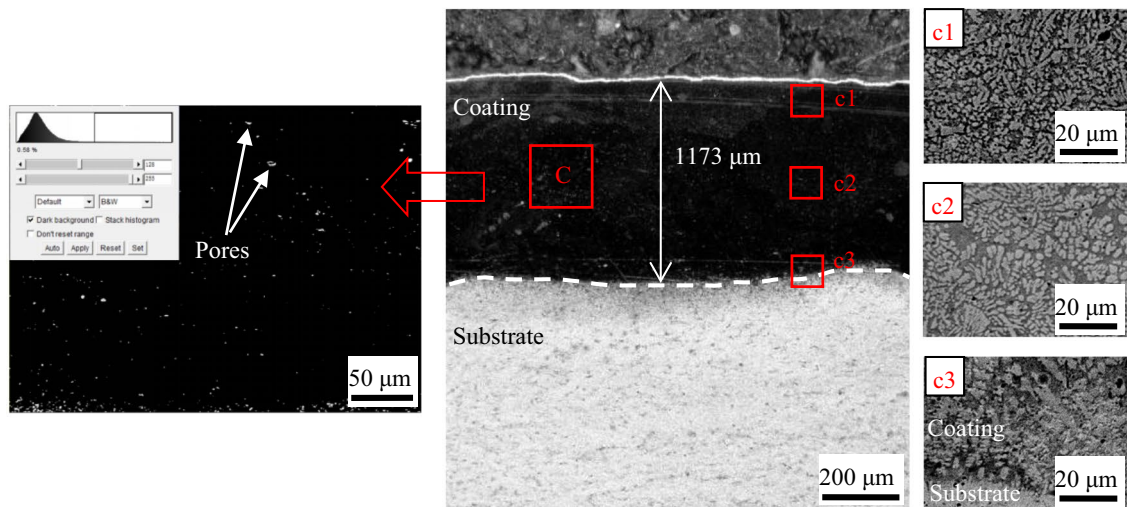Figure 9(a) shows the morphologies of worn track on the $WC-10Co4Cr-Al_2O_3-3\%La_2O_3$ coating. From the low

(a) WC−10Co4Cr−Al$_2$O$_3$−3%La$_2$O$_3$ coating

(b) WC−10Co4Cr−Al$_2$O$_3$−6%La$_2$O$_3$ coating

(c) WC−10Co4Cr−Al$_2$O$_3$−9%La$_2$O$_3$ coating

◀**Fig.5** Microstructure and porosity of $WC-10Co4Cr-Al_2O_3$ coating cross-sections with different La_2O_3 mass fractions

magnified image on the left, there were some parallel furrows on the worn track, which belonged to abrasive wear. From the high magnified image on the right, there were some micro-cracks on the worn track, and the debris was cut into the coating to form the furrows under the action of normal load due to its large grain size and uneven distribution of phases on the coating. In this case, the parallel furrows and cracks appeared on the worn track with the continuation of wear time, leading to generating abrasive debris and accelerating the wear loss of coating.

Figure 9(b) shows the morphologies of worn track on the $WC-10Co4Cr-Al_2O_3-6\%La_2O_3$ coating. There were a large number of parallel furrows on the wear track, indicating that the wear mechanism was abrasive wear. No cracks were found on the worn track, which was because the crack sensitivity [45] of coating decreased with the increase of La_2O_3 mass fraction.

Figure 9(c) shows the morphologies of worn track on the $WC-10Co4Cr-Al_2O_3-9\%La_2O_3$ coating. The abrasive debris was cut into the coating under the action of normal load, which left the furrows on the worn track, indicating that the wear mechanism was abrasive wear. Moreover, no cracks were found on the worn track, suggesting that the wear performance was improved with the increase of La_2O_3 mass fraction.

In summary, the wear resistance of $WC-10Co4Cr-Al_2O_3$ coatings enhanced with the increase of La_2O_3 mass fraction, indicating that the grain refinement and dispersion strengthening by the addition of La_2O_3 were the main factor of affecting the friction-wear performances.

Line scan analysis of worn tracks

In order to further analyze the wear mechanism, line scan analysis was used to investigate the distributions of chemical elements on the worn tracks. The line scanned position of worn track on the $WC-10Co4Cr-Al_2O_3-3\%La_2O_3$ is shown in Fig. 10(a). And the line scan results are shown in Fig. 10(b), where the W, C, Co, Cr, and Fe were detected on the worn track. The W on the worn track was lower than the unworn coating, while the Cr and Fe were opposite, and the C was uniformly distributed on the worn track. This was because the WC and other hard phase distributions on worn track were not uniform, and the WC phase on the worn track was worn away layer by layer. In the friction process, the WC was peeled off and formed abrasive debris on the zones with the less WC in the wear process, where more Fe–Cr binders were exposed on the worn track.

Figure 11 (a) shows the line scanned position of worn track on $WC-10Co4Cr-Al_2O_3-6\%La_2O_3$ coating. The line scan results are shown in Fig. 11(b), where the W, C, Co, Cr, and Fe were detected on the worn track. This was because the WC and other hard phase distributions on the worn track were relatively uniform with the increase of La_2O_3 mass fraction, which played the role of strengthening second phase to improve the wear resistance of coating [38]. However, the uneven distributed zones of WC and other hard phases were peeled off to form abrasive debris, which led to more exposure of Fe–Cr binders.

The line scanned positions of worn tracks on the $WC-10Co4Cr-Al_2O_3-9\%La_2O_3$ are shown in Fig. 12(a). And the line scan results are shown in Fig. 12(b), where the W, C, Co, Cr, Fe, and O were detected. The contents of W, C, Co, Cr, and Fe on the worn track were not changed significantly than the unworn coating, indicating that the wear degree was not serious. The line scan analysis also showed that the O distribution of on the worn track was higher than that of unworn coating. This was because the La_2O_3 promoted the formation of oxide film on the coating surface to prevent the coating from further oxidation. When the oxides on the worn track were worn away, more oxides of Al_2O_3, La_2O_3, $LaAlO_3$, and $LaCoO_3$ were exposed on the worn track, which led to the O content on the worn track higher than that on the unworn coating.

Wear mechanism

Figure 13(a) shows the wear model of $WC-10Co4Cr-Al_2O_3-3\%La_2O_3$ coating. The uneven distribution of hard phases gathered together on the worn track, resulting in high porosity and large grain sizes of coating. In the wear test, the abrasive debris was produced between the coating and the tribo-pair, which were pressed into the worn track and moved along the tangent direction to generate the furrows and micro-cracks. Under the action of cyclic load, the micro-cracks extended along the grain boundary on the worn track [46], which expanded and connected with each other. The hard particles were peeled off to form new abrasive debris, which participated in the wear process again.

Figure 13(b) shows the wear model of $WC-10Co4Cr-Al_2O_3-6\%La_2O_3$ coating. Compared with former coating, the aggregation phenomenon of hard phases on the coating surface was reduced. Most of hard phases were uniformly distributed on the coating, which played a role of dispersion strengthening to improve the coating hardness. Moreover, the La_2O_3 was easily gathered on the grain boundary [27], dislocation, and other defects, which played the role of grain refinement to hinder the movement
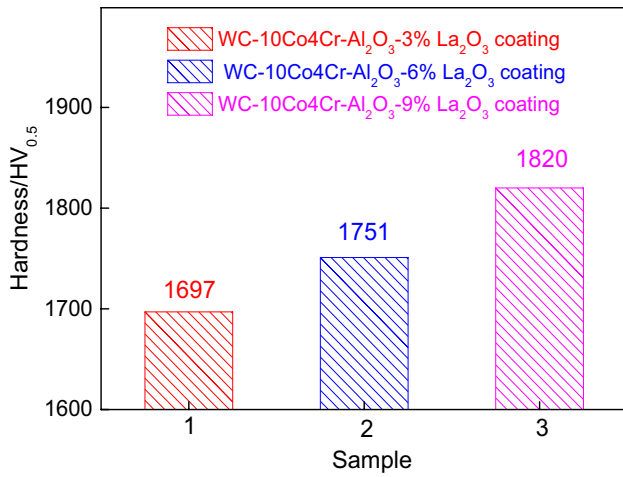
Fig.6 Hardness of $WC-10Co4Cr-Al_2O_3$ coating surfaces with different La_2O_3 mass fractions

of dislocation and the grain growth. Therefore, the hardness and wear resistance of coating was improved than the former coating.

Figure 13(c) shows the wear model of $WC-10Co4Cr-Al_2O_3-9\%La_2O_3$ coating. The microstructure of coating was further improved with the increase

of La_2O_3 mass fraction, resulting in the decrease of porosity and grain size. According to the strengthening theory [29], the strengthening effect of hard phase was enhanced with the decrease of grain size. The results showed that the fine dispersed hard phases enhanced the effects of grain reinforcement and dispersion strengthening, resulting in the increase hardness and wear resistance of coatings. Therefore, the worn track became narrow and shallow.

The worn track of $WC-10Co4Cr-Al_2O_3-3\%La_2O_3$ coating had the micro-cracks, while the other two coatings did not form the micro-cracks, which was explained by the Hall–Patch equation [28] of grain reinforcement theory. The equation is showed as follows:

$$\sigma = \sigma_0 + Kd^{-1/2} \tag{7}$$

where σ was the yield strength/MPa; σ_0 was the single-grain yield strength/MPa; K was the constant; and d was the grain size/μm.

From Eq. (7), the small grain size meant the high yield strength. The grain sizes of $WC-10Co4Cr-Al_2O_3$ coatings decreased with the increase of La_2O_3 mass fraction; i.e., the yield strength of coatings increased with the increase of La_2O_3 mass fraction, and the capability of deformation resistance also increased. Therefore, the
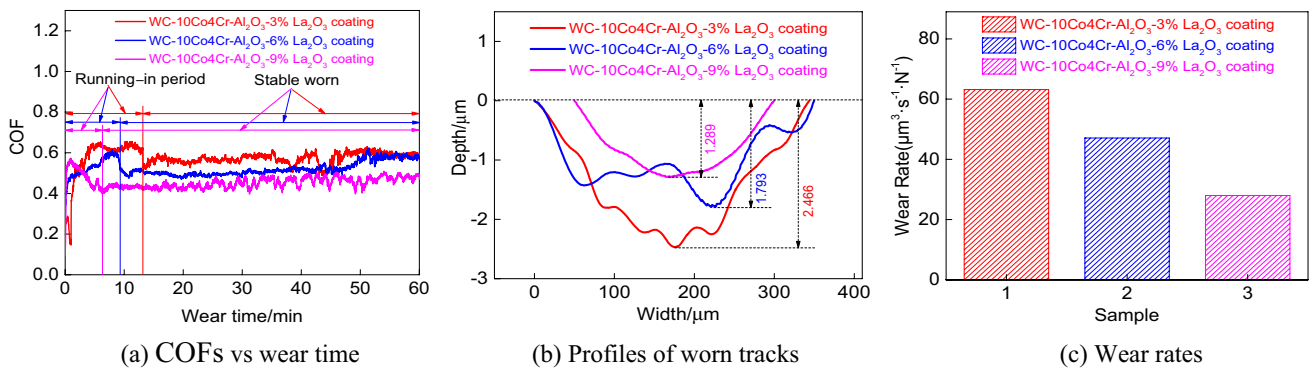

(a) COFs vs wear time

(b) Profiles of worn tracks

(c) Wear rates

Fig.7 COFs vs wear time, profiles of worn tracks, and wear rates of $WC-10Co4Cr-Al_2O_3$ coatings with different La_2O_3 mass fractions

(a) $WC-10Co4Cr-Al_2O_3-3\%La_2O_3$

(b) $WC-10Co4Cr-Al_2O_3-6\%La_2O_3$
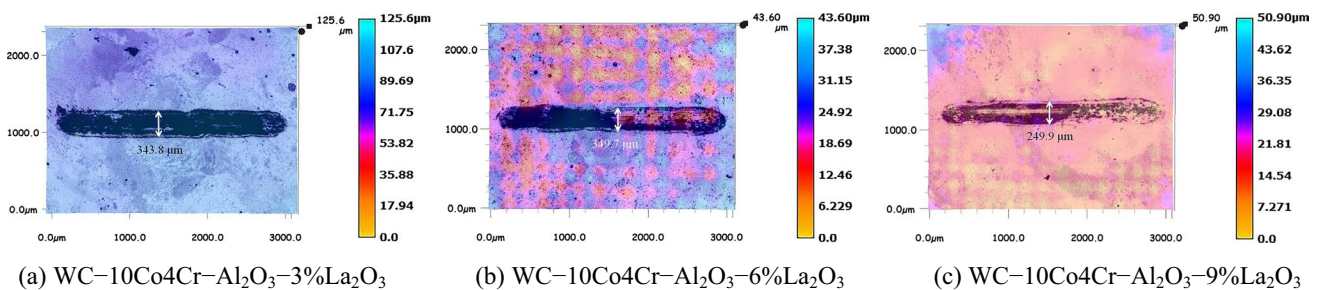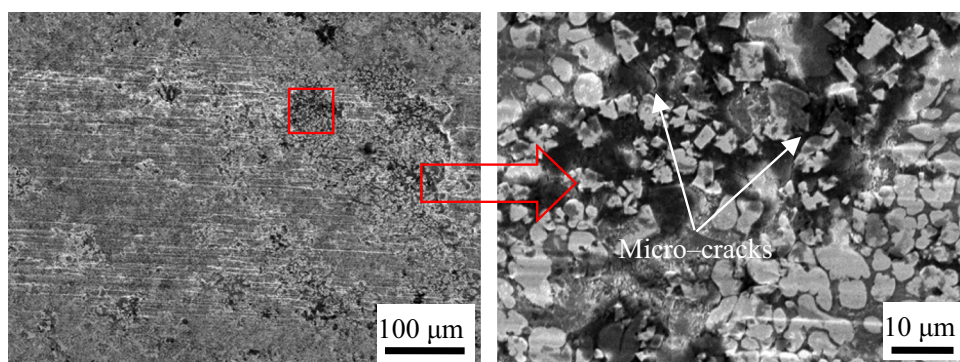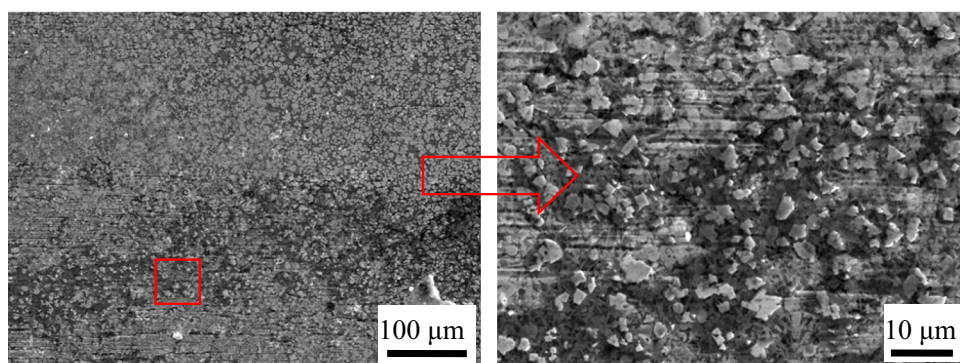
(c) $WC-10Co4Cr-Al_2O_3-9\%La_2O_3$

Fig.8 Overall images of worn tracks on $WC-10Co4Cr-Al_2O_3$ coatings with different La_2O_3 mass fractions
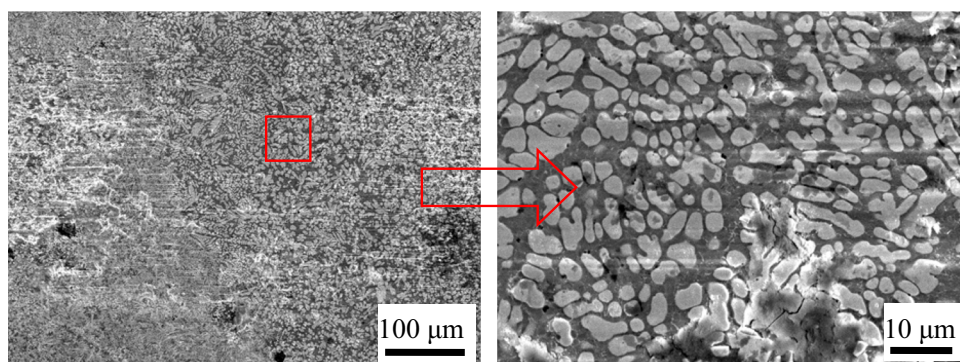
Fig.9 Morphologies of worn tracks on $WC-10Co4Cr-Al_2O_3$ coatings with different La_2O_3 mass fractions

(a) On WC−10Co4Cr−Al₂O₃−3%La₂O₃ coating

(b) On WC−10Co4Cr−Al₂O₃−6%La₂O₃ coating

(c) On WC−10Co4Cr−Al O −9%La₂O₃ coating

cracks were reduced when the coating was subjected to external force, which effectively improved the wear resistance of coating.

In this case, the aggregations of hard phases were effectively prevented on the $WC-10Co4Cr-Al_2O_3$ coating with the increase of La_2O_3 mass fraction, and the effect of grain reinforcement was more obvious, which played the role of dispersion enhancement. As a result, the hardness and wear resistance of $WC-10Co4Cr-Al_2O_3$ coatings increased by the addition of La_2O_3.

Fig.10 Line scan analysis of worn track of $WC-10Co4Cr-Al_2O_3-3\%$ La_2O_3 coating
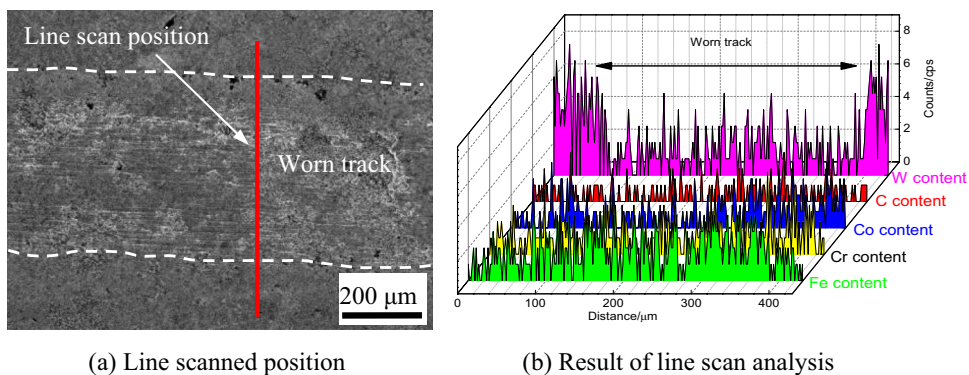
(a) Line scanned position

(b) Result of line scan analysis

Fig.11 Line scan analysis of worn track of $WC-10Co4Cr-Al_2O_3-6\%$ La_2O_3 coating

(a) Line scanned position

(b) Result of line scan analysis

Fig.12 Line scan analysis of worn track of $WC-10Co4Cr-Al_2O_3-9\%$ La_2O_3 coating

(a) Line scanned position

(b) Result of line scan analysis
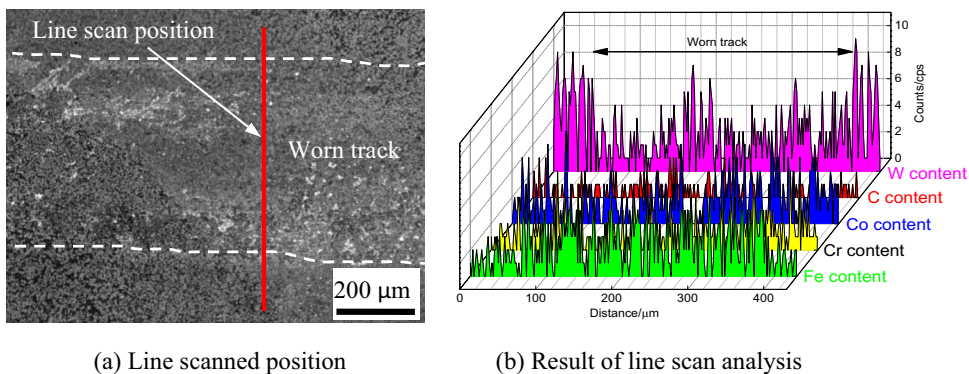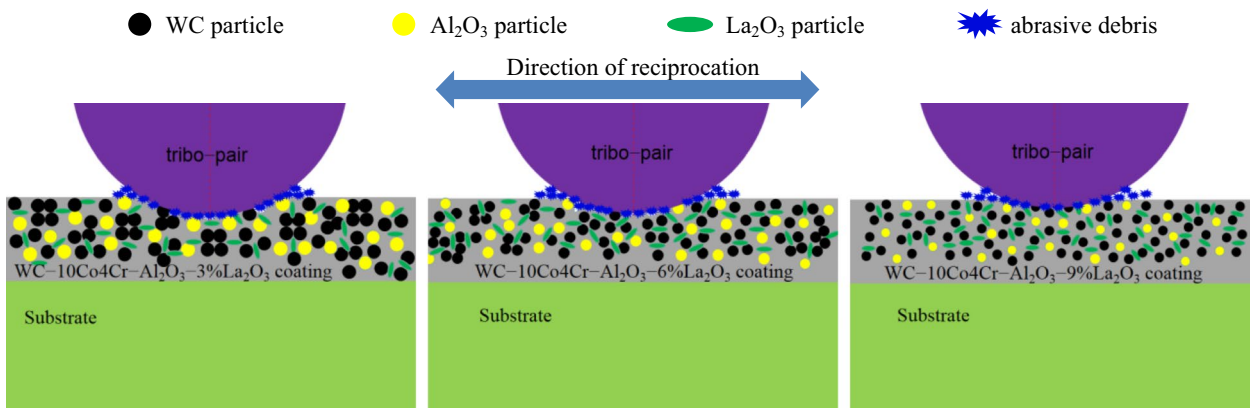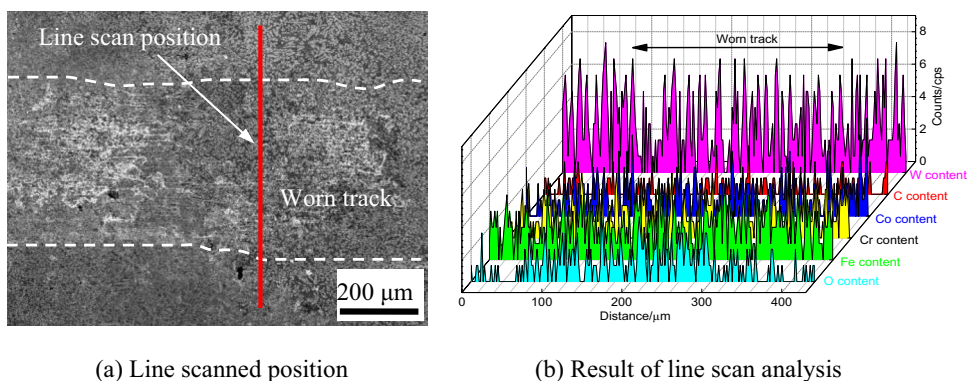
(a) $WC-10Co4Cr-Al_2O_3-3\%La_2O_3$ coating (b) $WC-10Co4Cr-Al_2O_3-6\%La_2O_3$ coating(c) $WC-10Co4Cr-Al_2O_3-9\%La_2O_3$ coating

Fig.13 Sketch of wear models on $WC-10Co4Cr-Al_2O_3$ coatings with different La_2O_3 mass fractions

Conclusions

(1) The La_2O_3 reinforced $WC - 10Co4Cr - Al_2O_3$ coatings are composed of WC, W_2C, Al_2O_3, La_2O_3, $LaAlO_3$, Fe–Cr, AlP_3Si, $LaCoO_3$, and LaP phases, and the surface hardness of $WC - 10Co4$ $Cr - Al_2O_3 - 3\%La_2O_3$, $- 6\%La_2O_3$ and $- 9\%La_2O_3$ coatings is 1697 ± 21, 1751 ± 32, and 1820 ± 27 $HV_{0.5}$, respectively, showing that the hardness of $WC - 10Co4Cr - Al_2O_3$ coatings increases with the increase of La_2O_3 mass fraction.

(2) The average COFs of $WC - 10Co4Cr - Al_2O_3 - 3\%La_2O_3$, $- 6\%La_2O_3$, and $- 9\%La_2O_3$ coatings are 0.57, 0.52, and 0.46, respectively, which decrease with the increase of La_2O_3 mass fraction, showing that the addition of La_2O_3 effectively improves the friction performance of $WC - 10Co4Cr - Al_2O_3$ coating.

(3) The wear rates of $WC - 10Co4Cr - Al_2O_3 - 3\%La_2O_3$, $- 6\%La_2O_3$, and $- 9\%La_2O_3$ coatings are 63.18, 47.1, and 27.99 $\mu m^3 \bullet s^{-1} \bullet N^{-1}$, respectively. The wear resistance of $WC - 10Co4Cr - Al_2O_3 - 9\%La_2O_3$ is the best among the three kinds of coatings, and the wear mechanism is abrasive wear.

Declarations

Conflict of interest The authors declare no competing interests.

References

1. Wu, B.Y., Liu, P., Wang, X.Z., Zhang, F., Deng, L.M., Duan, J., Zeng, X.Y.: Effect of laser absorption on picosecond laser ablation of Cr12MoV mold steel, 9Cr18 stainless steel and H13A cemented carbide. Opt. Laser. Technol. **101**, 11–20 (2018)

2. Anandkumar, R., Almeida, A., Vilar, R.: Microstructure and sliding wear resistance of an Al−12w.t%Si/TiC laser clad coating. Wear **282–283**, 31–39 (2012)

3. Tan, H., Luo, Z., Li, Y., Yan, F., Duan, R., Huang, Y.: Effect of strengthening particles on the dry sliding wear behavior of $Al_2O_3 - M_7C_3$/Fe metal matrix composite coatings produced by laser cladding. Wear **324–325**, 36–44 (2015)

4. Hong, S., Wu, Y., Wang, B., Zhang, J., Lei, Q.: The effect of temperature on the dry sliding wear behavior of HVOF sprayed nanostructured WC−CoCr coatings. Ceram. Int. **43**(1), 458–462 (2016)

5. González, M.A., Rodríguez, E., Mojardín, E., Jiménez, O., Guillen, H., Ibarra, J.: Study of the erosive wear behaviour of cryogenically and tempered WC−CoCr coating deposited by HVOF. Wear **376–377**, 595–607 (2017)

6. Song, B., Murray, J.W., Wellman, R.G., Pala, Z., Hussain, T.: Dry sliding wear behaviour of HVOF thermal sprayed WC−Co−Cr and WC−Cr_xC_y−Ni coatings. Wear **442–443**, 203114 (2019)

7. Voorwald, H.J.C., Souza, R.C., Pigatin, W.L., Cioffi, M.O.H.: Evaluation of WC−17Co and WC−10Co−4Cr thermal spray coatings by HVOF on the fatigue and corrosion strength of AISI 4340 steel. Surf. Coat. Technol. **190**(2–3), 155–164 (2005)

8. Shi, J.Z., Ge, Y., Kong, D.J.: Microstructure, dry sliding friction performances and wear mechanism of laser cladded WC−10Co4Cr coating with different Al_2O_3 mass fractions. Surf Coat Technol. **406**, 126749 (2021)

9. Zhao, T., Cai, X., Wang, S.X., Zheng, S.A.: Effect of CeO_2 on microstructure and corrosive wear behavior of laser−cladded Ni/WC coating. Thin Solid Films **379**(1–2), 128–132 (2000)

10. Li, X., Mo, Y., Yu, X., Liu, W.: Influence of La_2O_3 on tribological properties of laser clad Ni−base alloy coating for ZL108. Lubr. Eng. **3**, 103–104 (2006)

11. Kong, W.C., Li, K.M., Hu, J.: Effects of laser power on microstructure and friction−wear performances of direct energy deposited ZrO_2−8%Y_2O_3−NiCoCrAl coatings on Ti6Al4V alloy. Optics Laser Technol. **142**, 107214 (2021)

12. Sharma, S.P., Dwivedi, D.K., Jain, P.K.: Effect of La_2O_3 addition on the microstructure, hardness and abrasive wear behavior of flame sprayed Ni based coatings. Wear **267**(5), 853–859 (2008)

13. Wang, X., Rong, J., Yao, Y.H., Zhang, Y.N., Zhong, Y., Feng, J., Yu, X.H., Zhan, Z.L.: La doping inhibits stress production at the grain boundaries in Ni−WC coating. J. Alloy. Compd. **753**, 688–694 (2018)

14. Xie, M., Zhang, S., Li, M.: Comparative investigation on HVOF sprayed carbide−based coatings. Appl. Surf. Sci. **273**, 799–805 (2013)

15. Lysenko, E., Nikolaev, E., Vlasov, V., Surzhikov, A.: Microstructure and reactivity of Fe_2O_3−Li_2CO_3−ZnO ferrite system ball−milled in a planetary mill. Thermochim. Acta. **664**, 100–107 (2018)

16. Zhou, J.L., Kong, D.J.: Friction−wear performances and oxidation behaviors of Ti_3AlC_2 reinforced Co−based alloy coatings by laser cladding. Surf Coat Technol. **408**(25), 126816 (2021)

17. Mahony, O., Yue, S., Turdean-Ionescu, C., Hanna, J.V., Smith, M.E., Lee, P.D.: Jones JR Silica−gelatin hybrids for tissue regeneration: inter−relationships between the process variables. J Sol-Gel Sci Technol **69**(2), 288–298 (2014)

18. Kong, W.C, Yu, Z., Hu, J.: Effect of carburizing treatment on microstructural, mechanical and tribological performances of Cr doped DLC coating deposited on Ti6Al4V alloy. Ceram Int https://doi.org/10.1016/j.ceramint.2021.08.355

19. Yuan, J.L., Yu, L.F., Li, F., Zhou, F.F., Zhao, P., Hang, W.: Study on the inherent correlations of the material properties for silicon nitride ceramic balls. Adv. Mater. Res. **1136**, 515–519 (2016)

20. Hu, M., Tang, J.C., Chen, X.G., Ye, N., Zhao, X.Y., Xu, M.M.: Microstructure and properties of WC−12Co composite coatings prepared by laser cladding. T. Nonferr. Metal. Soc. C. **30**(04), 1017–1030 (2020)

21. Zhang, Y., Yu, F.Y., Hao, S.Z., Dong, F.Y., Xu, Y., Geng, W.B., Zhang, N.N., Gey, N., Grosdidier, T., Dong, C., Lavacchi, A.: Evolution of nanostructure and metastable phases at the surface of a HCPEB−treated WC−6%Co hard alloy with increasing irradiation pulse numbers. Coatings **7**(11), 178 (2017)

22. Öksüz, K.E., Kumruoğlu, L.C., Tur, O.: Effect of sicp on the microstructure and mechanical properties of sintered distaloy DC composites. Procedia Mater. Sci. **11**, 49–54 (2015)

23. Simsir, M., Öksüz, K.E.: Effects of sintering temperature and addition of Fe and B_4C on hardness and wear resistance of

diamond reinforced metal matrix composites. J. Superhard Mater. **35**, 369–382 (2013)

24. Mishra, T.K., Kumar, A., Sinha, S.K.: Experimental investigation and study of HVOF sprayed WC−12Co, WC−10Co−4Cr and Cr_3C_2−25NiCr coating on its sliding wear behaviour. Int J Refract Meter H. **94**, 105404 (2021)

25. Qiu, X., Tariqc, N.U.H., Qi, L., Tang, J.R., Cui, X.Y., Du, H., Wang, J.Q., Xiong, T.Y.: Influence of particulate morphology on microstructure and tribological properties of cold sprayed A380/Al_2O_3 composite coatings. Int. J. Refract. Meter. H. **44**, 9–18 (2020)

26. Li, M.Y., Han, B., Wang, Y., Pu, K.J.: Effects of La_2O_3 on the microstructure and property of laser cladding Ni−based ceramic coating. Optik **130**, 1032–1037 (2017)

27. Kim, Y.J., Kim, S.W., Kim, H.B., Park, C.N., Choi, Y.I., Park, C.J.: Effects of the precipitation of secondary phases on the erosion−corrosion of 25% Cr duplex stainless steel. Corros. Sci. **152**, 202–210 (2019)

28 Zhu, Lh., Li, Y.S., Shi, S.J., Yan, Z.W.: Chen J Morphology and kinetics evolution of nanoscale phase in Fe−Cr alloys under external strain. Nanomaterial. **9**(2), 294 (2019)

29. Liu, X.B., Meng, X.J., Liu, H.Q., Shi, G.L., Wu, S.H., Sun, C.F., Wang, M.D., Qi, L.H.: Development and characterization of laser clad high temperature self−lubricating wear resistant composite coatings on Ti−6Al−4V alloy. Mater. Design **55**(6), 404–409 (2014)

30. Sharma, S.: Erosive Wear study of rare earth−modified HVOF−sprayed coatings using design of experiment. J. Therm. Spray. Technol. **21**(1), 49–62 (2012)

31. Wang, Y.Y., Li, C.J., Ohmori, A.: Examination of factors influencing the bond strength of high velocity oxy−fuel sprayed coatings. Surf. Coat. Technol. **200**(9), 2923–2928 (2006)

32. Yang, X.W., Li, W.Y., Yu, S.Q., Xu, Y.X., Hu, K.W., Zhao, Y.B.: Electrochemical characterization and microstructure of cold sprayed AA5083/Al_2O_3 composite coatings. J. Mater. Sci. Technol. **59**, 117–128 (2020)

33. Sun, X., Wang, Y., Li, D.Y.: Mechanical properties and erosion resistance of ceria nano−particle−doped ultrafine WC−12Co composite prepared by spark plasma sintering. Wear **301**(1–2), 406–414 (2013)

34. Zhu, R.D., Li, Z.Y.: Microstructure and properties of the low−power−laser clad coating on magnesium alloy with different amount of rare earth addition. Appl. Surf. Sci. **353**, 405–413 (2015)

35. Jia, Y.J., Li, H.J., Yao, X.Y., Sun, J.J., Zhao, Z.G.: Long−time ablation protection of carbon/carbon composites with different La_2O_3 content modified ZrC coating. J. Eur. Ceram. Soc. **38**(4), 1046–1058 (2018)

36. Gao, Y.X., Yi, J.: Effect of La_2O_3 addition on microstructure and wear behavior of electrospark deposited Ni−based coatings. Surf. Rev. Lett. **20**(6), 1350060 (2013)

37. Silva, D.M.R., Gargarella, P., Gustmann, T., Filho, W.J.B., Kiminami, C.S., Eckert, J., Pauly, S.: Bolfarini C Laser surface remelting of a Cu−Al−Ni−Mn shape memory alloy. Mater Sci and Eng A-Struct. **661**, 61–67 (2016)

38. Zhou, C.Y., Zhao, S.S., Wang, Y.B., Liu, F.L., Gao, W.Y., Lin, X.H.: Mitigation of pores generation at overlapping zone during laser cladding. J. Mater. Process Technol. **216**, 369–374 (2015)

39. Chen, H.P., Cheng, J.G., Zhang, M.L., Chen, W.C., Wei, B.Z., Chen, P.Q., Luo, L.M., Wu, Y.C.: Effect of rare earth oxide addition on the microstructure and properties of ultrafine grain W−20Cu composites. Rare. Metal. Mater. Eng. **47**(9), 2626–2630 (2018)

40. Zhu, Y.C., Yukimura, K., Ding, C.X., Zhang, P.Y.: Tribological properties of nanostructured and conventional WC−Co coatings deposited by plasma spraying. Thin Solid Films **388**(1–2), 77–282 (2001)

41. Li, Y.L., Yang, Q.X., Zhao, Y.H.: Thermodynamics of modifying effect of rare earth oxide on inclusions in hardfacing metal of medium−high carbon steel. J. Rare Earth **20**(4), 291–294 (2002)

42. Cho, S.J., Hockey, B.J., Lawn, B.R., Bennison, S.J.: Grain−size and R−curve effects in the abrasive wear of alumina. J. Am. Ceram. Soc. **72**(7), 1249–1252 (2010)

43. Nascimento, M.P., Souza, R.C., Pigatin, W.L., Voorwald, H.J.C.: Effects of surface treatments on the fatigue strength of AISI 4340 aeronautical steel. Int. J. Fatigue. **23**(7), 607–618 (2001)

44. Nascimento, M.P., Souza, R.C., Miguel, I.M., Pigatin, W.L., Voorwald, H.J.C.: Effects of tungsten carbide thermal spray coating by HP/HVOF and hard chromium electroplating on AISI 4340 high strength steel. Surf. Coat. Technol. **138**(2–3), 113–124 (2001)

45. Zhao, N., Tao, L., Guo, H., Zhang, M.Q.: Microstructure and wear resistance of laser cladded Ni−based coatings with nanometer La_2O_3 addition. Rare. Metal. Mater. Eng. **46**(8), 2092–2096 (2017)

46. Han, T., Deng, C.M., Zhang, X.F., Liu, Q.: A model of splats deposition state and wear resistance of WC−10Co4Cr coating. Ceram. Int. **44**(4), 4230–4236 (2018)